Bangladesh J. Bot. **53**(3): 835-847, 2024 (September) Special DOI: https://doi.org/10.3329/bjb.v53i30.76631

VEGETATION MONITORING IN MINING AREA USING CANOPY REFLECTANCE AND LANDSAT8 OLI IMAGE

PAN WU[1], LING CHEN[2], TAO WANG[1], KUN WANG[3*], RUNQING TIAN[1] AND QUAN FU[1]

College of Land Engineering, Chang'an University, Xi'an 710054, Shaanxi, China

Keywords: Leaf Angle Distribution, Reflectivity, Vegetation monitoring, NDVI, Copper Stress Vegetation Index

Abstract

The aim of this study was to find out the vegetation monitoring in mining areas which is of great significance in grasping the ecological environment status of mining areas. As the first target of spectral reflection, the vegetation canopy directly affects the results of spectral reception. Leaf Angle Distribution (LAD) is a key canopy structural parameter, which directly determines the amount of solar radiation intercepted by the canopy. Taking the relationship between the effect of leaf inclination angle on vegetation canopy reflectance and NDVI as an entry point, the study monitored and analyzed the vegetation in Dexing mining area, China, from 2013 to 2018 by NDVI, based on which the Copper Stress Vegetation Index (CSVI), which is applicable to the narrow wavelength band of remote sensing imagery, was evaluated whether it could be applied to the wide wavelength band. Results showed that the NDVI value of the horizontal distribution is significantly higher than that of other leaf inclination distributions, and the NDVI in the direction of the horizontal distribution was 0.82, while the NDVI in the direction of the hi-straight distribution was 0.75; the NDVI of the mining area decreased gradually with the increase of the area of the mining area, and the correlation coefficients of the two groups of CSVI based on the wide and narrow bands ware not large, which is not suitable for the vegetation monitoring by using the Landsat8 OLI imagery. Wide band is less applicable for vegetation monitoring.

Introduction

The canopy structure, as the composition of the top space of the vegetation community, directly affects the utilization of light energy by the vegetation, and affects the radiation exchange and water and air exchange of the plant community. Therefore, the study of vegetation canopy is an important part of vegetation remote sensing (Russell *et al.* 1989, Gastellu-Etchegorry *et al.* 1996, Zhang *et al*. 2017, Zhang *et al.* 2022) Leaf Angle Distribution (LAD) is a key canopy structure parameter, which directly determines the amount of solar radiation intercepted by the canopy, also plays a decisive role in the direction and size of incident solar radiation, and is an important factor (Masek *et al.* 2020) determining the photosynthetic efficiency of vegetation. For remote sensing sensors, LAD affects the radiation transfer process of photons in the canopy, and then affects the canopy reflectance detected by the sensor. Therefore, it is of great significance for vegetation remote sensing to study the impact of LAD on canopy reflectance (Sesnie *et al.* 2008, Hunter *et al.* 2010, SONdergaard *et al*. 2010).

As one of the world's largest mining countries, China's mining development is the third largest in the world (Chun-jing *et al* 2016, Zhang *et al.* 2018). While generating huge economic benefits and acquiring mineral resources, the pollution of the environment caused by the long-standing crude development of mineral resources is a problem that should not be ignored, and it has a great impact on the safety of people's lives and properties as well as on the sustainable development of the society.

*Author for correspondence: <497486844@qq.com>. [1]Shaanxi Provincial Land Engineering Construction Group Land Survey Planning and Design Institute, Xi'an 710075, China. [2]Xi'an Northwest Non-ferrous Geophysical and Chemical Exploration Group Co., Ltd, Xi'an 710068, China. [3]Institute of Land Engineering and Technology, Shaanxi Provincial Land Engineering Construction Group Co., Ltd, Xi'an 710075, Shaanxi, China.

The Dexing Copper Mine in China is the largest open pit copper mine in Asia and a super-large porphyry copper mine in China, which started open pit mining in 1958, and the vegetation in the vicinity of the mine is severely stressed by copper and other heavy metals, and the change of the vegetation in the mine area is of great significance to the ecological environment of the area and is an important indicator for ecological environment monitoring in the mine area (Enaruvbe and Atafo 2019, Lixin S *et al.* 2023).

The first part of this study is to quantify the changes in the total area of the mine (including the area of tailings ponds, etc.) and the changes in the vegetation near the mine from 2013 to 2018, using the Dexing copper mine as the study area.

The research on environmental monitoring of the mining area has never stopped, and there are studies on soil spectrum, water spectrum, atmospheric spectrum and vegetation spectrum (Carmichael *et al*. 2014, QI *et al.* 2020, Zhao *et al.* 2024). Among them, the method of reflecting vegetation status through vegetation index is very common. In hyperspectral remote sensing spectral analysis, the information through band synthesis is much more than that of single band, which has the effect of "1+1>2", so it is mostly used to design vegetation index. Commonly used vegetation indexes include NDVI (Normalized Difference Vegetation Index), DVI (Difference Vegetation Index) and RVI (Ratio of Vegetation Index). These vegetation indexes are based on the strong absorption of red light and the strong reflection of near-infrared light in the vegetation reflection spectrum. The second part of this study is based on the proposed CSVI for narrow band applications (Copper Stress Vegetation Index) (Yang 2019). In literature the correlation between CSVI and copper content in plants based on crop information such as wheat and soybean as well as soil information was higher than the other four existing vegetation indexes (NDVI, DVI, PRI, REP), and the universality of CSVI was verified using cabbage and rape as tests (Liu *et al.* 2016, Badgley *et al*. 2017, Sun *et al.* 2023, Zhang and Hu 2023). The existing vegetation monitoring indexes all consider spectral reflectance, but the effect of leaf angle on canopy reflectance is ignored in spectral analysis.

Therefore, this study takes the monitoring of vegetation change in the mining area as the research object, and the Landsat8 OLI image as the data source. By analyzing the impact of leaf inclination on the canopy reflectance, the quantitative calculation of the total area of the mining area and the vegetation change near the mining area from 2013 to 2018 is carried out, in order to explore the rule of vegetation change in the mining area, reflect the changes in the ecological environment of the mining area, and provide some technical support for the monitoring of the ecological environment of the mining area.

Materials and Methods

Dexing Copper Mine, located in Dexing City (28°41′ N, 117°44′ E), in the north of Shangrao City, Jiangxi Province (Fig. 1) , is the largest open-pit copper mine in Asia, with the annual output ranking first in China and second in the world. The total geographical area areas of these two city are 22737 km^2. It is a super large porphyry copper mine in China, including cinnabar, Tongchang and Fujiawu copper mines (Liu *et al.* 2022). The copper ore is shallow, high in content and large in reserves, which is suitable for open pit mining. Open pit mining began in 1958. It is an important nonferrous metal base (Liu *et al.* 2022) with world advanced level in China due to its good ore wash ability, small stripping ratio and multiple comprehensive uses of elements.

Data source comes from geospatial data cloud (http://www.gscloud.cn) Landsat8 OLI multispectral data. Seasonal differences have a great impact on the vegetation coverage of the mining area. Autumn and summer are the most vigorous seasons for vegetation growth, so the images of these two seasons are also the best time for dynamic monitoring and assessment

(DiMiceli *et al.* 2021). Due to the limitation of cloud amount and time of remote sensing images in the study area, most of the images could not be used. Finally, the data near February and August 2013-2018 were used to achieve the comparison of different years and the same period as far as possible. The hyperspectral image data used for comparative analysis is the Hyperion image in 2003. The characteristics of remote sensing images include their spatial, temporal and spectral characteristics, and the geographic location information is very important for remote sensing images, and when images acquired by different sensors or at different times in the same study area are to be comprehensively analyzed, they must be placed in the same geographic coordinate system in order to be processed in a meaningful way.

Fig. 1. Location of the study area**.**

The following methodologies have been proceed:

(1) Geometric registration. The Landsat8 image downloaded from the geospatial data cloud has been geometrically coarse corrected, so this work is not required. However, the Hyperion image needs to be geometrically registered according to other registered images in the study area, so the first step of Hyperion image operation is geometric registration. Due to the low requirements for the accuracy of geographical location in this study, it is not necessary to use topographic maps for geometric precision correction, as long as the two are relatively matched.

(2) Cropping. The Hyperion image used is a cropped image that includes a certain range of vegetation around the Dexing Copper Mine. The image boundary is used as the clipping vector to crop the Landsat8 image to get the study area of the same area.

Radiometric calibration refers to the process of converting the DN value originally recorded by the sensor into the radiance at the entrance pupil or the apparent reflectance at the top of the atmosphere. Atmospheric correction refers to the process of reducing or eliminating the impact of atmospheric reflection, scattering and absorption during the transmission of electromagnetic waves, and correcting the radiometric calibration data to obtain the true ground reflectance.

The radiometric calibration tool in ENVI and FLAASH Atmosphere Correction tool in ENVI are used for radiometric calibration and atmospheric correction of Landsat8 OLI images.

Leaf inclination refers to the angle between the normal to the ventral surface of the leaf blade and the zenith axis, i.e., the angle between the leaf blade veins and the horizontal plane (Fig. 2), and is a concept that is specific to a single leaf. While for the vegetation canopy, which is generally studied, the LAD, LAD One can use a density distribution function that $f(\theta_L, \emptyset_L)$ to characterize, among other things θ_L and $\emptyset_L$ are the inclination and azimuth of the leaf blades, respectively. Where, for horizontal distribution of canopy blades, the θ_L were all 0°, and the

canopy foliage at the hi straight distribution, the θ_L. Most of them were distributed between 0° and 30°, and only a relatively small number of blades had leaf inclinations greater than 30°, azimuth $\emptyset_L$. All are randomized LAD. Different from vegetation, it can be roughly idealized into six types: flat type, straight type, inclined type, extreme type, uniform type and spherical distribution type. The LAD of some vegetation, such as sunflowers, will change with the rise and fall of the sun and wind conditions in a day. DART model takes the leaf inclination distribution as an input parameter and there are various distribution types available, e.g., the uniform (uniform type distribution), spherical (spherical distribution), erectophile (hi straight distribution), planophile (horizontal distribution), etc.

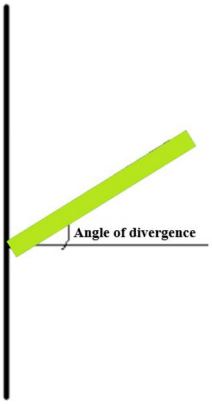

Fig. 2. Schematic diagram of leaf inclination angle (the green flat plate in the diagram is the leaf blade).

DART model, namely discrete anisotropic radiative transfer model, is a computer simulation model. It can simulate any number of spectral bands (such as visible light to thermal infrared band) in the optical field, radiation budget and remote sensing data (radiation image, lidar waveform and photon count) in some earth scenes, as well as different solar incidence angles (Ω s), atmosphere and observation directions (Ω v). DART model divides the scene into a rectangular cell matrix to build a module for simulating larger scenes. These cells are parallel to each other, and their optical properties are represented by a single scattering phase function, which is generally directly input into the model or calculated from the optical properties and structural properties of the elements in the cell. The input parameters of DART model can be divided into the following three categories: 1) geometric and lighting parameters: zenith angle of sensor observation, solar zenith angle, ratio of direct solar radiation to total solar radiation, etc. 2) Optical parameters: leaf wax refractive index, vegetation reflectance, vegetation transmittance, background (soil) reflectance, etc.) Canopy structure parameters: leaf angle distribution (LAD), leaf area index (LAI), crown size, etc. (Cai *et al*. 2020). As the main object of this study, leaf inclination distribution mainly affects the area of light canopy/background and shadow canopy/background (Formula 1) by changing the amount of canopy radiation interception, and then affects the canopy reflectance.

The canopy reflectance received by the sensor is equal to the area-weighted sum of the four component reflectance, i.e., the

$$R = R_T \cdot P_T + R_G \cdot P_G + R_{ZT} \cdot Z_T + R_{ZG} \cdot Z_G \quad (1)$$

P_T is the light canopy, the Z_T is the shaded canopy, the P_G is the light background, the Z_G is a shaded background, the R_T is the area of the light canopy, the R_{ZT} is the area of

the shaded canopy, the R_G is the area of the lighted background, the R_{ZG} is the area of the shaded background.

Detection of Changes in Mining and Vegetation were conducted as below:

(1) Mine change detection

The expansion of the mining area will become a factor in the change of the degree of metal stress on the vegetation. Therefore, first analyze whether there is any change in the mining area of Dexing Copper Mine. Firstly, the mining area can be extracted from the remote sensing image by visual interpretation. Because the tailings pond and waste rock yard are also the parts that affect the vegetation, they are also included in the total area of the mining area. Next, the mining area of each image can be quantitatively obtained by using the computational geometry in ArcMap, and the dynamic change effect of the mining area in a long time series can be seen through superposition display.

(2) Vegetation change detection

Because the NDVI value of vegetation is higher than that of other features, the vegetation area of each image can be well extracted by using the NDVI threshold setting method. First, use NDVI to set the threshold value to make mask file, and then use the mask to process the original image. Only the image map of vegetation area can be obtained. The threshold value of the same month in each year must be kept the same in order to have comparative value. The growth status of vegetation in different months is also different, so appropriate thresholds should be selected to extract.

The pixel value of vegetation in the mask file is 1, and the pixel value of non-vegetation is 0. Subtracting the image mask files of the same month in different years can get three results: 0 (no change), -1 (vegetation becomes non-vegetation), and 1 (non-vegetation becomes vegetation), and by comparing the change of these three values, the change of vegetation cover from 2013 to 2018 can be obtained.

The corresponding three bands required by CSVI can be found directly in hyperspectral data, but not in multispectral data. Instead, the required band results can only be obtained by replacing or interpolating adjacent bands. The Green (0.56) band in Landsat8 OLI image is used to replace the R_{550}, replaced by NIR (0.86) band R_{850} Since there is no reflectance data of 700nm waveband, the values obtained by inverse distance weight interpolation of Red (0.65) and NIR (0.86) wavebands are used to replace the values in the above formula R_{700}. The formula is:

B3 = 0.76 x b1 + 0.24 x v2 (2)

The formula b1, b2, b3 red band (0.65), NIR band (0.86) R_{700}.

On the basis of the vegetation area obtained in the previous section, use the Band Math tool of ENVI to obtain the CSVI. At the same time, perform the same processing on the hyperspectral data after geometric registration to obtain the CSVI of wide band and the CSVI of hyperspectral data Hyperion image. Take the Landsat8 image in June 2014 as an example, use the Layer Stacking tool of ENVI to synthesize the CSVI of June 2014 and the CSVI of Hyperion image into a single layer, and then use the 2D Scatter Plot tool of ENVI to see the scatter plot of the two images and visually display the correlation.

Scatter map is only a qualitative view of the correlation from the distribution of the two, and cannot reflect quantitatively. Therefore, this paper also uses MATLAB to randomly select 10000 sample pixels, remove the pixels whose pixel value is NaN (that is, the null value in the non vegetation area), and then calculate the correlation coefficient and significance level of the two groups of CSVI to quantitatively get the description of the quality of linear correlation.

Results and Discussion

In this paper, the effect of leaf inclination distribution on canopy reflectance is studied by using DART model to simulate canopy reflectance. First, input the vegetation structure parameters, vegetation biochemical parameters, air/soil parameters and other parameters into the model except the leaf inclination distribution (Baniya *et al*. 2019), and set the parameters within a reasonable range as shown in Table 1.

Table 1 DART Model Input Parameters.

Parameters	Parameters values
Sun azimuth (°)	0
Sun zenith angle (°)	30
Mean temperature (K)	300
Band (near-infrared/red/blue/green) (nm)	800/670
Leaf reflectance (near infrared/red/blue/green)	0.49/0.048
Leaf transmittance (near infrared/red/blue/green)	0.41/0.043
Soil reflectance (near infrared/red/blue/green)	0.41/0.043
Number of trees	160
Leaf area index of the scene	4.50
Crown type ellipsoid	ellipsoid
Height of the trunk (m)	1
Canopy radius (m)	0.50
Canopy density 0.72	0.72
Scene size (m^2)	10x10

Run DART model to simulate canopy reflectance, process the results and draw a two-dimensional broken line chart of canopy reflectance changes with observed zenith angle under different leaf inclination distribution (Fig. 3). The specific results and analysis are as follows:

As can be seen in Fig. 3, the five curves have the same trend and show a "herringbone", and all of them have peaks when the zenith angle of the sensor observation is -30°, which is known as the "hot spot phenomenon" in the field of optical remote sensing, i.e., the sensor receives the strongest terrestrial radiation when the sensor is in the same direction as the sun. This phenomenon is called "hot spot phenomenon" in the field of optical remote sensing, that is, when the sensor is located in the same direction with the sun, the sensor receives the strongest ground radiation. Although the five curves of canopy reflectance with the zenith angle observed by the sensor have the same trend, there are obvious numerical differences in the curves in the figure, indicating that the distribution of leaf inclination angle does have a greater impact on the canopy reflectance. The quantitative analysis shows that the top curve in the figure is the simulation result of horizontal distribution, and the canopy reflectance in the direction of "hot spot" is 0.698, while the bottom curve, i.e., the canopy reflectance in the direction of "hot spot" in the simulation result of straight distribution, is only 0.533, both of which have the same trend with the zenith angle observed by the sensors. 0.533, the relative difference between the two "hot spot" direction canopy reflectance reached 31%, and the absolute difference reached 0.165, while the rest of the leaf inclination distribution simulation results in the two, the difference is also more obvious, so it can be seen that the leaf inclination distribution has a very big impact on the canopy reflectance.

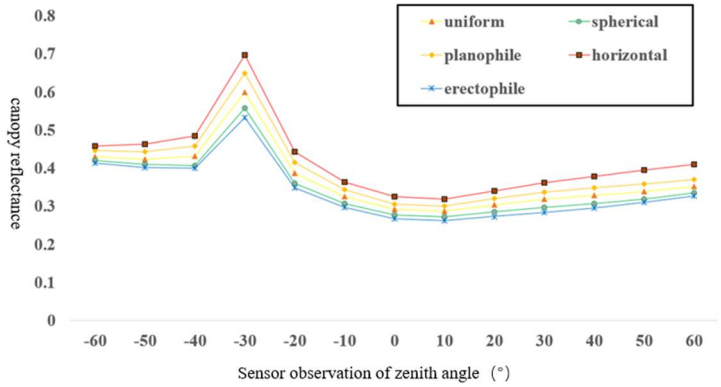

Fig. 3. The effect of leaf inclination distribution on canopy reflectance in the near-infrared band (the negative sign in the horizontal coordinate indicates backward scattering and the positive sign indicates forward scattering).

From the above, this is due to the fact that in the horizontal distribution case, the scene within the sensor's viewing angle consists mainly of the light canopy, the component in Eq. (2), the $R_T \cdot P_T$ values play a dominant role in canopy reflectance, and because canopy reflectance in the near-infrared band is modeled, leaf reflectance is much greater than background (soil) reflectance, thus a larger component $R_T \cdot P_T$ results in a larger canopy reflectance R. On the contrary, when the leaf inclination distribution is straight like, the light crown area is the smallest, and the sensor view is mostly the light background, thus the components $R_G \cdot P_G$ dominate the values of canopy reflectance R, due to the soil reflectance in the near infrared band □□Smaller, so the weight $R_G \cdot P_G$, the value is very small, so the canopy reflectance R is small. For the six leaf inclination distributions studied in this paper, the light canopy area observed by the sensor is horizontal>botanical>uniform>spherical>erectophile. Combined with the above analysis, canopy reflectance R: horizontal>botanical>uniform>spherical>erectophile will appear, which is completely consistent with the DART model simulation results shown in Fig. 4.

Fig. 4 simulates the influence of leaf inclination distribution on canopy reflectance in red light band. It can be seen that the curve height distribution in this figure is just opposite to that in Fig. 3. This is because the red-light band is the radiation "absorption zone" of vegetation, and the leaf reflectivity is small, while the soil reflectivity is relatively large. When the leaf inclination distribution is straight like, the light crown area is small, and the light background area is large. The main components that affect the canopy reflectivity R in Formula (2). The value of R is larger, so the simulated canopy reflectance R is larger. On the contrary, the canopy reflectance of horizontal distribution is small, and that of other leaf inclination distribution is between the two.

Vegetation index is a combination of reflectance of certain specific bands. In the field of remote sensing, vegetation index has been widely used to qualitatively and quantitatively evaluate vegetation cover and its growth vitality. Among them, NDVI (Normalized Vegetation Index) is a hotspot in the field of vegetation remote sensing research at home and abroad in recent years. NDVI=(NIR-R)/(NIR+R), which is the combination of near-infrared reflectance and red-light reflectance. Through the processing and data analysis of DART simulation results in the near infrared band and red-light band, it is found that LAD also has a greater impact on the NDVI index. The specific results and analysis are as follows:

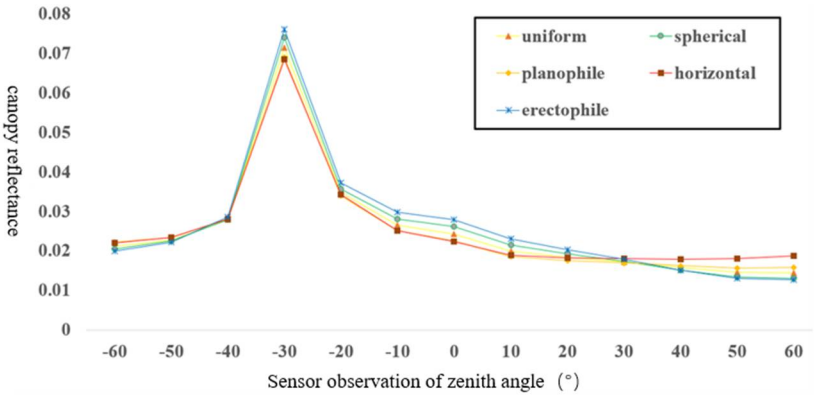

Fig. 4 Influence of leaf inclination distribution on canopy reflectance in the red-light band (the negative sign in the horizontal coordinate indicates backward scattering and the positive sign indicates forward scattering).

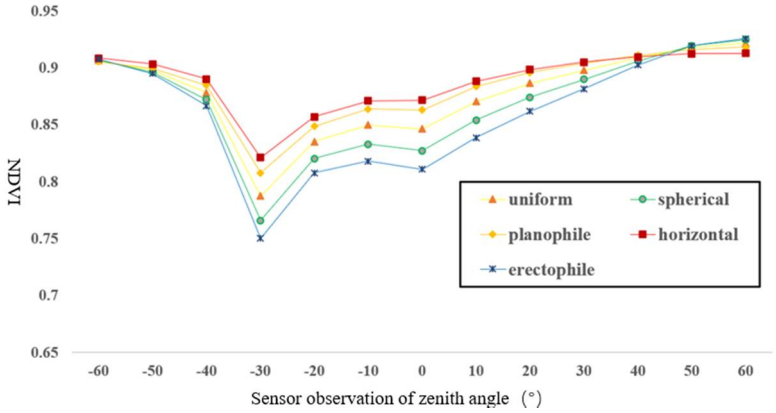

Fig. 5. Influence of Leaf Inclination Distribution on NDVI (abscissa negative sign indicates backward scattering, positive sign indicates forward scattering)

It can be seen from Fig. 5 that the NDVI values corresponding to different leaf inclination distributions are large, which indicates that the input parameters of DART model are all in an appropriate range, and the vegetation coverage and health status in the simulation scene are good. However, there are significant numerical differences between the five curves in the figure. Among them, the NDVI value of horizontal distribution is significantly higher than the simulation results of other leaf dip distributions. The NDVI in the "hot spot" direction of horizontal distribution is 0.82, while the NDVI in the "hot spot" direction of straight like distribution is 0.75, with a relative difference of 10%. This is because when the leaf dip distribution of the canopy is horizontal, the interception amount of the canopy to radiation will increase, which is equivalent to increasing the vegetation coverage, resulting in a larger NDVI. The main function of NDVI is to test the coverage of green vegetation in the scene, so as to detect and estimate the plant biomass. Fig. 5 shows the specific values of NDVI under different LADs, which is helpful to analyze the growth of green plants in the scene and retrieve parameters such as plant biomass.

Changes in mining and vegetation areas were as below:

(1) Mining areas

This paper selects one image every year, which is in August 2013, June 2014, April 2015, March 2016, May 2017 and April 2018. The remote sensing interpretation results using ArcGIS are shown in Fig. 1. According to the interpretation results, the statistical area for 6 years is shown in Table 2

Table 2 Mining area statistics, 2013-2018.

Year of remote sensing images	Area mined (m^2)
2013	22232850
2014	23436749
2015	24076321
2016	25453248
2017	25530553
2018	29033700

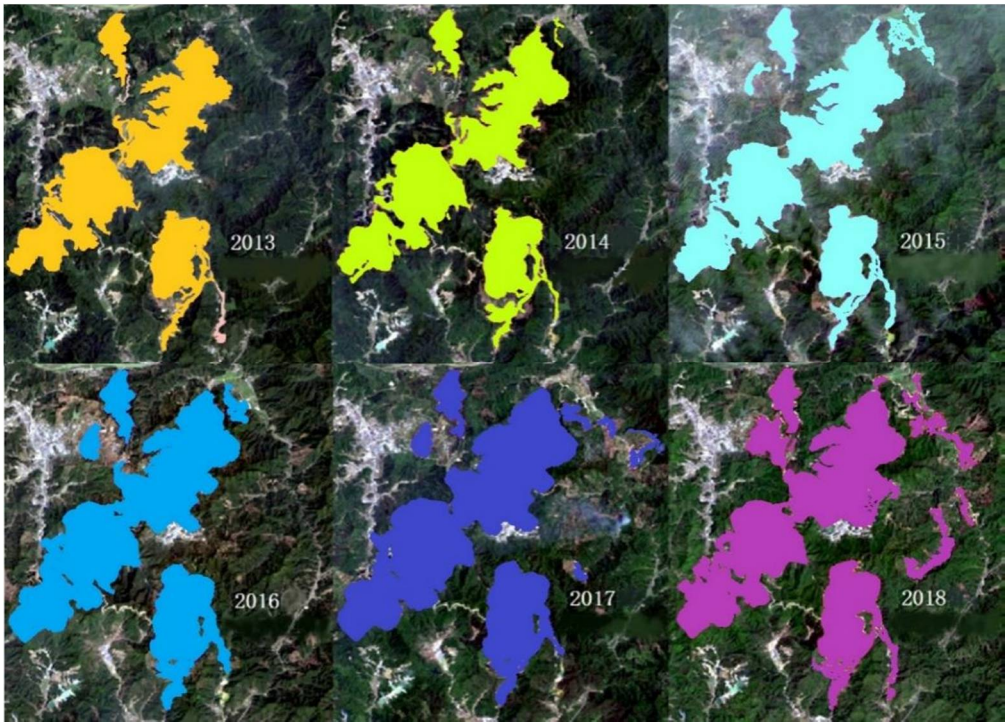

Fig. 6. 2013-2018 Deciphering results of the Dexing copper mine.

Thematic maps produced by overlaying the results of the six years of mine extraction are shown in Fig. 7, which visualizes the continued expansion of the mine area.

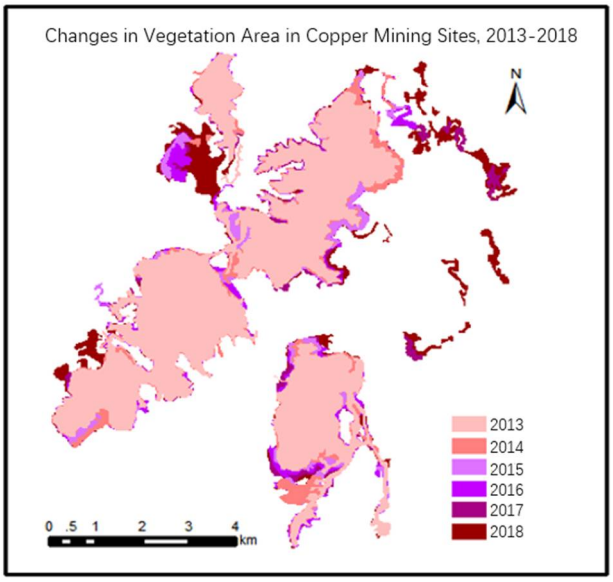

Fig. 7. Thematic map of changes in vegetation area at the Dexing Copper Mine, 2013-2018.

With the known results of increasing mine area, the study continued to examine the changes in vegetation in the mine area. Due to the limitations of image acquisition, the years that can be compared with similar months are restricted, the present study compared the statistical changes in the number of non-vegetated pixels of vegetation in February and April from 2014 to 2017(Table 3).

Table 3. Changes in the number of vegetated and non-vegetated image elements in February and April, 2014-2017.

Month of year	Vegetation - > non vegetation (a)	Non vegetation - > vegetation (b)	No change (c)
2014.2-2015.2	16077	29200	371929
2015.2-2016.2	18678	21564	376964
2016.2-2017.2	27913	16075	373218
2015.4-2016.4	10015	37389	369802
2016.4-2017.4	50528	8789	357889

The April 15 image is cloudy, which has a greater impact; (2) March 28, 16 is approximated as April in the calculation.

From the first three lines of data, the area of class a has become larger and larger, while the area of class b has been decreasing from 2014 to 2017. In particular, from 2016 to 2017, the area of class a is almost twice the area of class b, indicating that the image of the mining area is increasing. In combination with the above monitoring on the area of the mining area, it can be seen that the increase of the mining area may be an important factor affecting the vegetation change.

Wide band CSVI analysis was as below:

(1) ENVI 2D Scatter Plot

The scatter plot results of CSVI values of 12 Landsat multispectral images and hyperspectral images are shown in Fig. 8.

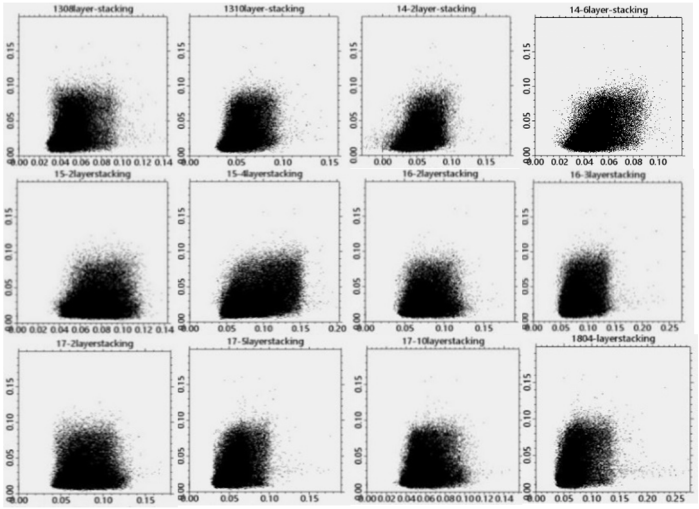

Fig. 8. Scatter map of CSVI values of multispectral and hyperspectral images (Notes: x-axis is the CSVI of Landsat8; y-axis is the CSVI of Hyperion).

From the above figure, the linear correlation is not so obvious that it is not easy to make a judgment, and the general view is that the correlation is weak, so the next operation of the correlation coefficient is indispensable.

(2) Calculation of Pearson correlation coefficient and significance by MATLAB

The correlation coefficient between CSVI of 12 images and CSVI of hyperspectral image obtained in MATLAB is shown in Table 4.

Table 4. Summary of linear correlation coefficients.

Landsat image	Correlation coefficient ρxy	P value	Landsat image	Correlation coefficient ρxy	P value
2013.08	0.4067	0.0000	2016.02	0.1699	0.0000
2013.10	0.4491	0.0000	2016.03	0.2474	0.0000
2014.02	0.4040	0.0000	2017.02	0.1553	0.0000
2014.06	0.4835	0.0000	2017.05	0.4982	0.0000
2015.02	0.2144	0.0000	2017.10	0.2505	0.0000
2015.04	0.3468	0.0000	2018.04	0.4962	0.0000

In general $|\rho X_y| > 0.8$ is called high correlation, when $|\rho X_y| < 0.3$, it is called low correlation, and other times it is medium correlation, and the P value of this calculation result is 0, indicating that the correlation coefficient is significant. According to the linear correlation coefficient

obtained, except for several images, the correlation coefficient obtained is close to 0.5, the correlation between other images and the CSVI of hyperspectral images is very poor. Therefore, it is concluded that the vegetation index CSVI based on narrow band is not suitable for wide band, at least because it is not suitable for unknown band based on the method of inverse distance weighting used in this paper.

Based on DART model, canopy reflectance was simulated and the result data was processed, and the influence of leaf inclination distribution on canopy reflectance was obtained. The following conclusions were obtained from the analysis of the results: 1) In the near infrared band, when the leaf inclination distribution is horizontal and flat, the canopy reflectance is significantly higher than the reflectance under other leaf inclination distribution. Especially in the near infrared band, the canopy reflectance in the horizontal distribution "hot spot" direction reached 131% of that in the straight distribution "hot spot" direction. On the contrary, in the red-light band, the canopy reflectance of the straight like distribution is significantly higher than that of other leaf inclination distributions, while the canopy reflectance of the horizontal distribution and the flat like distribution is lower; 2) Through the reflectance combination of the simulation results of near-infrared and red-light bands, it is found that LAD also has a greater impact on common vegetation indexes such as NDVI.

Based on the study of canopy reflectance, the quantitative calculation and analysis of vegetation index in the mining area were carried out. It was found that with the continuous increase of the mining area, the area of the area where vegetation disappeared was also increasing, indicating that the expansion of mining scale and the increase of mining area had a great impact on the destruction of plants, even destructive destruction of plants in some areas. In addition, in the research on the applicability of CSVI in wide band, the inverse distance weighted interpolation method is used to calculate the unknown band, and the correlation coefficients of two groups of CSVI based on wide band and narrow band are not large. The conclusion is that the applicability of CSVI in wide band is poor. However, other methods can be tried to deal with the problem of unknown band on the wide band, and the correlation can be compared. This leaf will be the next research direction.

Acknowledgements

The present work was funded by Inner scientific research project of Shaanxi Land Engineering Construction Group (DJNY-YB-2023-18, DJNY-YB-2023-28, DJNY-YB-2023-40, DJNY2024-16, DJNY2024-18, DJNY2024-33), Internal scientific research projects of Shaanxi Land Survey and Planning Institute, Shaanxi Provincial Land Engineering Construction Group Co., Ltd. in 2024 (KCNY2024-2, KCNY2024-4).

References

Badgley G, Field CB and Berry JA 2017. Canopy near-infrared reflectance and terrestrial photosynthesis. Sci. Adv. **3**(3): e1602244.

Baniya B, Tang Q, Xu X, Haile GG and Chhipi-Shrestha G 2019. Spatial and temporal variation of drought based on satellite derived vegetation condition index in Nepal from 1982-2015. Sensors **19**(2): 430.

Carmichael MJ, Bernhardt ES, Bräuer SL and Smith WK 2014. The role of vegetation in methane flux to the atmosphere: should vegetation be included as a distinct category in the global methane budget? Biogeochem. **119**(1): 1-24.

Chun-jing, Li LZ, Yu Z, Bing-hua Z and Xiao-li H 2016. Retrieval and analysis of grassland coverage in arid Xinjiang, China and five countries of Central Asia. Pratacultural Sci. **10**(5): 861-870.

Cai D, Ge Q, Wang X, Liu B, Goudie AS and Hu S 2020. Contributions of ecological programs to vegetation restoration in arid and semiarid China. Environ. Res. Lett. **15**(11): 114046.

DiMiceli C Townshend, Carroll M and Sohlberg R 2021. Evolution of the representation of global vegetation by vegetation continuous fields. Remote Sensing of Environ. **254**: 112271.

Enaruvbe GO and Atafo OP 2019. Land cover transition and fragmentation of River Ogba catchment in Benin City, Nigeria. Sustainable Cities and Soc. **45**: 70-78.

Gastellu-Etchegorry JP, Demarez V, Pinel V and Zagolski F 1996. Modeling radiative transfer in heterogeneous 3-D vegetation canopies. Remote Sensing of Environ. **58**(2): 131-156.

Hunter PD, Tyler AN, Willby NJ and Kelly A 2010. Mapping macrophytic vegetation in shallow lakes using the Compact Airborne Spectrographic Imager (CASI). Aquatic Conservation: Marine and Freshwater Ecosystems **20**(7): 717-727.

Lixin S, Wenquan X, Zhiying Z, Pei and Xueying L 2023. Multi-dimension evaluation of remote sensing indices for land surface phenology monitoring. National Remote Sensing Bulletin **27**(11): 2653-2669.

Liu Y, Ye Z, Jia Q, Mamat A and Guan H 2022. Multi-source remote sensing data for lake change detection in Xinjiang, China. Atmosphere **13**(5): 713.

Liu G, Wang Y, Chen Y, Tong X, Wang Y and Xie J 2022. Remotely monitoring vegetation productivity in two contrasting subtropical forest ecosystems using solar-induced chlorophyll fluorescence. Remote Sensing **14**(6): 1328.

Masek JG, Wulder MA, Markham B, McCorkel J, Crawford CJ and Storey J 2020. Landsat 9: Empowering open science and applications through continuity. Remote Sensing of Environ. **248**: 111968.

Qi Y, Zhang F, Chen R and Wang Y 2020. Vegetation coverage dynamics in northern slope of Tianshan Mountains from 2001 to 2015. Acta Ecologica Sinica **40**(11): 3677-3687.

Russell G, Marshall B, Jarvis PG 1989. Plant Canopies Their Growth. Cambridge: Cambridge University Press.

SONdergaard M *et al*. (2010). Submerged macrophytes as indicators of the ecological quality of lakes. Freshwater Biol. **55**(4): 893-908.

Sesnie SE, Johansson LS, Lauridsen TL, JØRgensen TB, Liboriussen L and Jeppesen E 2008. Integrating Landsat TM and SRTM-DEM derived variables with decision trees for habitat classification and change detection in complex neotropical environments. Remote Sensing of Environ. **112**(5): 2145-2159.

Yang L 2019. Study on Atmospheric Circulation Characteristics of Precipitation Anomalies in Arid Region of Central Asia. **2019:** GC53G-1258.

Zhang C, Ren H, Qin Q and Ersoy OK 2017. A new narrow band vegetation index for characterizing the degree of vegetation stress due to copper: the copper stress vegetation index (CSVI). Remote Sensing Letters **8**(6): 576-585.

Zhang Y, Duan H, Xi H, Huang Z, Tsou J and Jiang T 2022. Characterizing changes in land cover and forest fragmentation from multitemporal Landsat observations (1993-2018) in the Dhorpatan Hunting Reserve, Nepal. J. For Res. **33**(1): 159-170.

Zhang Y, Sharma S, Bista M and Li M 2018. Evaluation of the influence of aquatic plants and lake bottom on the remote-sensing reflectance of optically shallow waters. Atmosphere-Ocean **56**(4): 277-288.

Zhang SX and ZM Hu 2023. Long-term and fine-scale monitoring of net primary productivity in northwestern hainan based on remote sensing data. Remote Sensing Technol. Applica. **38**(6): 1413-1422.

Zhao X, Tan S, Li Y, Wu H and Wu R 2024. Quantitative analysis of fractional vegetation cover in southern Sichuan urban agglomeration using optimal parameter geographic detector model, China. Ecol. Indicat. **158**: 111529.

(Manuscript received on 22 March, 2024; revised on 28 September, 2024)